Highly efficient and controllable surface polariton beam splitters

Chong Shou[1] and Guoxiang Huang[1,2,3]

[1]*State Key Laboratory of Precision Spectroscopy, East China Normal University, Shanghai 200062, China*
[2]*NYU-ECNU Joint Institute of Physics, New York University at Shanghai, Shanghai 200062, China*
[3]*Collaborative Innovation Center of Extreme Optics, Shanxi University, Taiyuan 030006, China*

(Received 29 July 2019; revised manuscript received 17 October 2019; published 26 December 2019)

We propose a scheme to realize highly efficient and controllable surface polariton beam splitters with a hybrid system via the electromagnetically induced transparency (EIT) of quantum emitters doped near the interface between a metamaterial and a dielectric. By means of the destructive interference effects contributed by the EIT of the quantum emitters and by the electric-magnetic response of the metamaterial, we show that such beam splitters can work at very low light level and they have small quantum decoherence and low Ohmic loss; moreover, the propagation loss of the surface polaritons can be reduced further by using weak microwave fields and the dispersion effect of the surface polaritons can be balanced by using the EIT-enhanced Kerr effect. Therefore, the surface polariton beam splitters obtained here have high splitting efficiency and may be controlled actively. Our study opens a route not only for coherent and active control of low-loss surface polaritons but also for promising applications in optical information processing based on quantum hybrid systems.

DOI: 10.1103/PhysRevA.100.063844

I. INTRODUCTION

Optical beam splitter is one of the most basic optical devices to manipulate light, especially to split a single optical beam into two or more ones, which may or may not have the same power, polarization, wave vector, frequency, and so on. Except for tremendous applications in classical optical physics and engineering, optical beam splitters play also important roles in the study of quantum optics, relativity theory, quantum information, and many fields of quantum science and technologies [1–4].

In recent years, plasmonic metamaterials have earned a great deal of attention due to the growing demand on solid-state photonic integration for practical applications, and hence a transfer of conventional techniques of optical beam splitters to such materials is of great interest. In fact, up to now there have been various theoretical and experimental studies on surface polariton beam splitters (SPBS) based on plasmonic metamaterials [5–28]. However, most of them require high input power, have large Ohmic loss and low splitting efficiency, and cannot be controlled actively.

In the past 15 years, much attention has also been paid to the study of optical beam splitters based on atomic gases [29–40] via electromagnetically induced transparency (EIT), a typical quantum interference effect occurring in multilevel quantum emitters interacting with two or more laser fields [41]. Although such beam splitters have many advantages, they have large device size and need to fight against the movement of atoms, etc., and hence are hard to be miniaturized and integrated as necessary for practical applications.

In this work, we suggest a scheme for realizing highly efficient and controllable SPBS via EIT, which is drastically different from those reported in Refs. [5–40]. The system used is a hybrid one, where four-level quantum emitters are doped near the interface between a plasmonic metamaterial and a dielectric. We shall demonstrate that, due to the two types of destructive interference effects contributed respectively by the EIT of the quantum emitters and by the joint electric and magnetic responses of the metamaterial, such SPBS can work at very low light power, and they have small quantum decoherence and low Ohmic loss. Furthermore, the propagation loss of the surface polaritons (SPs) can be suppressed further by using weak microwave fields that couple three bottom levels of the quantum emitters, and the dispersion effect of the SPs can be canceled by exploiting the EIT-enhanced Kerr nonlinear effect. As a result, the SPBS with such a quantum hybrid system predicted here have high splitting efficiency and may be controlled actively. In addition, the scheme presented here can easily be generalized to realize surface polariton routers. Our study opens a way not only for the coherent and active control of low-loss surface polaritons, but also for the design of SPBS with high efficiency and controllability based on solid hybrid quantum systems, which can be made to have small device size and hence are promising for compact chip-integrated applications.

II. MODEL

We consider an interface consisting of a negative-index metamaterial (permittivity ε_1 and permeability μ_1) as the bottom plane and a dielectric (permittivity ε_2 and permeability μ_2) as the top plane [see Fig. 1(a)] [42–44]. Quantum emitters [45] (denoted by solid black dots) with four-level tripod-type configuration are dropped into a thin layer of the dielectric near the metamaterial-dielectric interface. A weak, pulsed probe laser field (with angular frequency ω_p) and the two strong continuous wave control laser fields (with angular frequencies ω_{c1} and ω_{c2}) are incident along the x direction of the interface. SPs are generated by the coupling

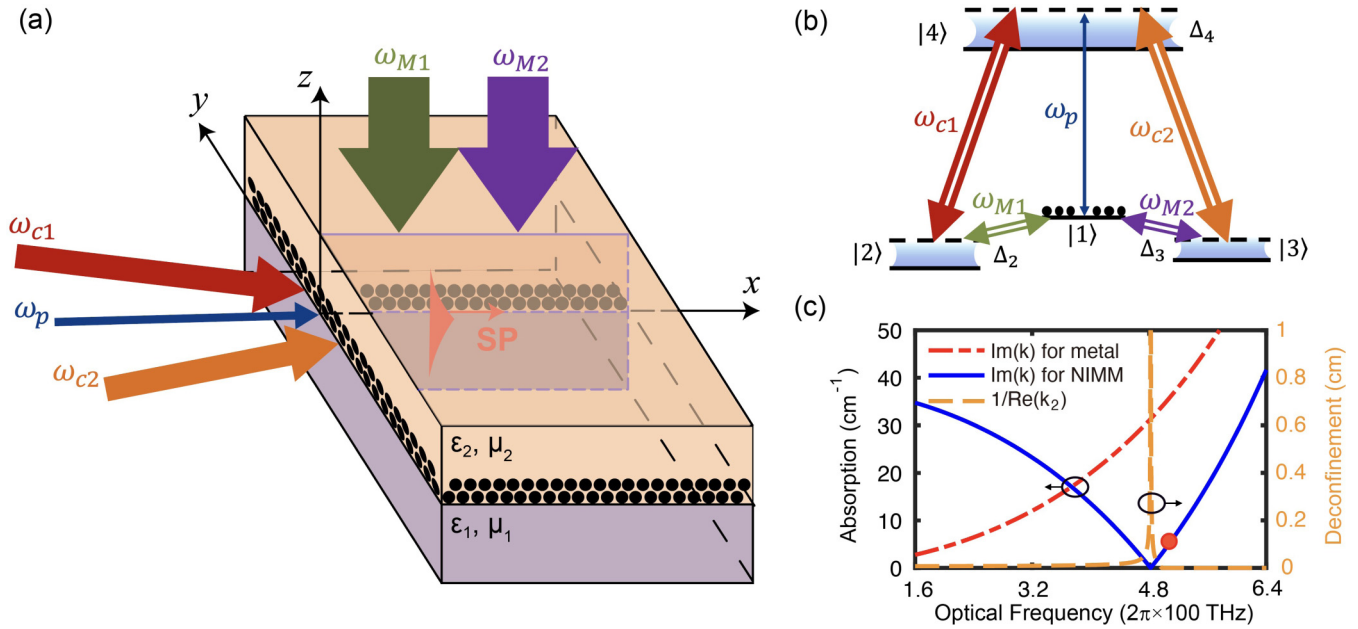

FIG. 1. (a) SP mode (red triangle) generated by incident probe field near the interface of the metamaterial (ε_1, μ_1) and the dielectric (ε_2, μ_2), propagating along x direction. Quantum emitters (solid black dots) are doped in the thin layer of the dielectric near the interface. The probe field (angular frequency ω_p) and two control fields (angular frequencies ω_{c1} and ω_{c2}) are incident along the interface; the two microwave fields (angular frequencies ω_{M1} and ω_{M2}) are incident along $-z$ direction. (b) The level diagram and excitation scheme of the four-level tripod-type quantum emitters; Δ_4 is the one-photon detuning; Δ_2 and Δ_3 are the two-photon detunings. The initial population is prepared at the ground state $|1\rangle$. (c) The absorption spectrum Im(k) of the SP for the metamaterial-dielectric interface (solid blue line) and for a metal-dielectric interface (dashed-solid red line). The dashed orange line denotes the deconfinement parameter $1/\mathrm{Re}(k_2)$ as a function of optical oscillating frequency ω_l. The solid red circle on the solid blue line is the selected one, where the SP has small Ohmic loss and strong spatial confinement along the z direction, simultaneously.

between the laser fields and the metamaterial-dielectric interface. Figure 1(b) shows the energy levels ($j = 1,\ 2,\ 3,\ 4$) and the laser excitation scheme of the quantum emitters, with Δ_4 [$\Delta_{2(3)}$] the one-photon (two-photon) detuning. The initial population of the quantum emitters is assumed to be prepared in the ground state $|1\rangle$. The system has two Λ-type EIT, with the energy levels $|1\rangle$, $|2\rangle$, $|4\rangle$, and the levels $|1\rangle$, $|3\rangle$, $|4\rangle$, respectively. We assume also that two weak continuous-wave microwave fields (with half Rabi frequencies Ω_{M1} and Ω_{M2}, respectively) respectively couple the bottom levels $|1\rangle \leftrightarrow |2\rangle$ ($|1\rangle \leftrightarrow |3\rangle$) [see Fig. 1(b)] used to provide a gain to suppress the propagation loss of SPs.

The metamaterial-dielectric interface supports both transverse magnetic (TM) and transverse electric (TE) modes. Due to the fast decay of the TE mode, here we consider only the TM one, which reads [43,44]

$$\mathbf{E}(\mathbf{r},t) = \begin{cases} (k\mathbf{e}_z + ik_1\mathbf{e}_x)\frac{c}{\varepsilon_1\omega_l}\sqrt{\frac{\hbar\omega_l}{\varepsilon_0 L_x L_y L_z}}a(\omega_l)e^{k_1 z + i(kx-\omega_l t)} + \text{c.c.} & (z<0), \\ (k\mathbf{e}_z - ik_2\mathbf{e}_x)\frac{c}{\varepsilon_2\omega_l}\sqrt{\frac{\hbar\omega_l}{\varepsilon_0 L_x L_y L_z}}a(\omega_l)e^{-k_2 z + i(kx-\omega_l t)} + \text{c.c.} & (z>0), \end{cases} \tag{1}$$

where $\mathbf{r} = (x,\ z)$ [46], $\mathbf{e}_x$ ($\mathbf{e}_z$) is the unit vector along the x (z) direction, ω_l is oscillating frequency, $k_\alpha^2 = k^2 - \omega_l^2\varepsilon_\alpha\mu_\alpha$ ($\alpha = 1, 2$) is the wave vector satisfying the relation $k_1\varepsilon_2 = -k_2\varepsilon_1$, $k = (\omega_l/c)[\varepsilon_1\varepsilon_2(\varepsilon_1\mu_2 - \varepsilon_2\mu_1)/(\varepsilon_1^2 - \varepsilon_2^2)]^{1/2}$ is the propagation constant of the SP mode in the absence of the quantum emitters, L_x and L_y are respectively lengths of the metamaterial-dielectric interface along x and y directions, and L_z is the effective length of z direction. Here we assume that the photon number of the all laser fields are much larger than unity and hence the quantity $a(\omega_l)$ (photon-number operator) can be taken as a constant number.

We assume that the metamaterial can be described by using complex macroparameters, i.e., the permittivity and the permeability, which are given by [42–44] $\varepsilon_1(\omega_l) = \varepsilon_\infty - \omega_e^2/[\omega_l(\omega_l + i\gamma_e)]$ and $\mu_1(\omega_l) = \mu_\infty - \omega_m^2/[\omega_l(\omega_l + i\gamma_m)]$, where ω_e and ω_m are electric and magnetic plasma frequencies of the metamaterial, γ_e and γ_m are corresponding decay rates, and ε_∞ and μ_∞ are background constants. The solid blue line in Fig. 1(c) is the imaginary part of the propagation constant k, i.e., Im(k), of the SP as a function of ω_l in the absence of the quantum emitters. We see that, comparing with conventional metal-dielectric interface (given by the dashed-solid red line), a significant suppression of the Ohmic loss occurs, which is due to the fact that there is a destructive interference between the electric and the magnetic responses of the metamaterial [42–44]. When plotting the figure, the

system parameters chosen are $\varepsilon_\infty = \mu_\infty = 1$, $\omega_e = 1.37 \times 10^{16}$ s^{-1}, $\gamma_e = 2.73 \times 10^{13}$ s^{-1} (as for Ag), $\omega_m = 3.21 \times 10^{15}$ s^{-1}, $\gamma_m = 10^{11}$ s^{-1}, $\varepsilon_2 = 1.3$, and $\mu_2 = 1$.

From Fig. 1(c) it seems that there is a possibility to achieve a complete suppression of the SP Ohmic loss. However, such complete suppression is unavoidably accompanied by a deconfinement of the SP along the interface, i.e., when $\mathrm{Im}(k) \to 0$, the deconfinement parameter $1/\mathrm{Re}(k_2)$ grows rapidly (see the dashed orange line). Therefore, one has to select an appropriate excitation frequency ω_l with a small deviation from the lossless point. In our study, the solid red circle on the solid blue line in the figure, corresponding to $\omega_l = 2\pi \times 495$ THz, is the selected one where the SP Ohmic loss can still be suppressed greatly and a strong SP confinement along the z direction can also be achieved simultaneously.

Due to the surface plasmonic resonance, the incident probe field will convert into the SP mode. For simplicity, we assume that the probe and control fields are coupled to the SP mode. Then the expression of the electric field of the system is given by $\mathbf{E}(\mathbf{r},t) = \sum_{l=p,c1,c2} \mathbf{u}_l(z)\xi_l(\mathbf{r},t)e^{i[k(\omega_l)x-\omega_l t]} + \text{c.c.}$, with $\mathbf{u}_l(z) = (c/\varepsilon_2\omega_l)[k(\omega_l)\mathbf{e}_z - ik_2(\omega_l)\mathbf{e}_x]\, e^{-k_2(\omega_l)z}$ and $\xi_l(\mathbf{r},t) = [\hbar\omega_l/(\varepsilon_0 L_x L_y L_z)]^{1/2}\, a(\omega_l,\mathbf{r},t)$. Under rotating-wave approximation, in the presence of the quantum emitters and absence of the microwave fields the Hamiltonian of the system in the interaction picture is given by

$$\hat{H}_{\text{int}} = -\hbar\left\{\sum_{j=1}^{4}\Delta_j|j\rangle\langle j| + [\zeta_p(z)\Omega_p|4\rangle\langle 1| + \zeta_{c1}(z)\Omega_{c1}|4\rangle\langle 2| + \zeta_{c2}(z)\Omega_{c2}|4\rangle\langle 3| + \text{H.c.}]\right\}, \quad (2)$$

where $\Delta_1 = 0$, $\Delta_4 = \omega_p - (E_4 - E_1)/\hbar$, $\Delta_2 = \omega_p - \omega_{c1} - (E_2 - E_1)/\hbar$, and $\Delta_3 = \omega_p - \omega_{c2} - (E_3 - E_1)/\hbar$, with E_j the eigenenergy of the state $|j\rangle$; $\Omega_p(\mathbf{r},t) = \xi_p(\mathbf{r},t)(\mathbf{e}_p \cdot \mathbf{p}_{41})/\hbar$ and $\Omega_{c1(c2)} = \xi_{c1(c2)}(\mathbf{e}_{c1(c2)} \cdot \mathbf{p}_{42(43)})/\hbar$ are, respectively, the half Rabi frequencies of probe and control fields, with $\mathbf{p}_{ij}$ the electric dipole matrix element associated with the transition from state $|i\rangle$ and state $|j\rangle$. Since the control fields are strong, $\xi_{c1(c2)}$ can be taken as constants during the evolution of the probe field. Since $\omega_p \approx \omega_{c1} \approx \omega_{c2}$, one has $\zeta_{c1}(z) \approx \zeta_{c2}(z) \approx \zeta_p(z) = \mathbf{u}_p(z) \cdot \mathbf{e}_{14} \equiv \zeta(z)$. The motion of the quantum emitters is governed by the optical Bloch equation

$$\frac{\partial\sigma}{\partial t} = -\frac{i}{\hbar}[\hat{H}_{\text{int}},\sigma] - \Gamma[\sigma], \quad (3)$$

where σ is a 4×4 density matrix and Γ is a respective relaxation matrix characterizing the spontaneous emission and dephasing in the system. The explicit expressions of Eq. (3) for matrix elements σ_{jl} ($j,\ l = 1,\ 2,\ 3,\ 4$) are presented in Appendix A.

The electric polarization intensity of the quantum emitters in the system can be expressed by $\mathbf{P}(\mathbf{r},t) = \mathcal{N}_{\text{QE}}(z)[\mathbf{p}_{14}\sigma_{41}e^{i(k_p x-\omega_p t)} + \mathbf{p}_{24}\sigma_{42}e^{i(k_{c1}x-\omega_{c1}t)} + \mathbf{p}_{34}\sigma_{43}e^{i(k_{c2}x-\omega_{c2}t)} + \text{c.c.}]$, where $\mathcal{N}_{\text{QE}}(z)$ is the quantum emitter density. For simplicity, we assume that $\mathcal{N}_{\text{QE}}(z) = \mathcal{N}_a$ for $0 < z < z_0$ and zero for $z < 0$ and $z > z_0$, where $\mathcal{N}_a$ is a constant and $z_0 = 2$ μm is the thickness of the doped interface. Hence the Maxwell equation describing the evolution of the SP is given by

$$i\left(\frac{\partial}{\partial x} + \frac{n_2^2}{n_{\text{eff}}c}\frac{\partial}{\partial t}\right)\Omega_p + \langle\kappa_{14}(z)\tilde{\sigma}_{41}\rangle = 0, \quad (4)$$

where $\kappa_{14}(z) \equiv \mathcal{N}_{\text{QE}}(z)|\mathbf{p}_{14}|^2\omega_p/(2n_{\text{eff}}\hbar\varepsilon_0 c)$, $\sigma_{41} \equiv \tilde{\sigma}_{41}\zeta(z)$, $\langle\psi\rangle \equiv \int_{-\infty}^{+\infty} dz|\zeta(z)|^2\psi/[\int_{-\infty}^{+\infty} dz|\zeta(z)|^2]$ (ψ is an arbitrary of z), and n_2 and $n_{\text{eff}} \equiv ck/\omega_p$ are respectively the refractive indices of the dielectric and the effective refractive index of the system in the absence of the quantum emitters.

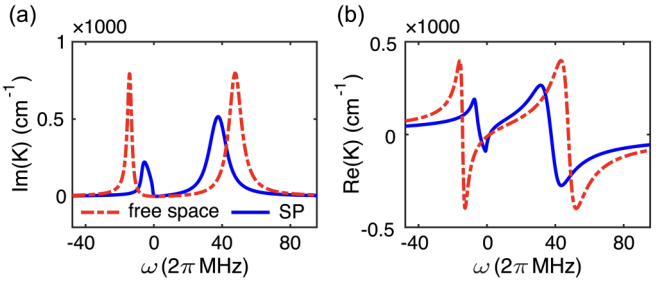

FIG. 2. Linear dispersion relation K of the SP as a function of ω [47]. (a) The imaginary part $\mathrm{Im}(K)$. (b) The real part $\mathrm{Re}(K)$. In both panels, the solid blue lines are for the SP and the dashed red lines are for free space (i.e., the metamaterial-dielectric interface is absent).

III. RESULTS AND DISCUSSION

A. Linear dispersion relation of the SP

For a weak probe pulse, the evolution of the SP is linear. From Maxwell-Bloch (MB) Eqs. (3) and (4) we obtain the solution for Ω_p with the form $\Omega_p = F\, e^{i[K(\omega)x-\omega t]}$ [47], where F is constant and $K(\omega)$ is the linear dispersion relation

$$K(\omega) = \frac{n_2^2\omega}{n_{\text{eff}}c} - \left\langle\kappa_{41}(z)\frac{(\omega+d_{21})(\omega+d_{31})}{D}\right\rangle, \quad (5)$$

with $D = -|\zeta(z)\Omega_{c1}|^2(\omega+d_{31}) - |\zeta(z)\Omega_{c2}|^2(\omega+d_{21}) + (\omega+d_{41})(\omega+d_{21})(\omega+d_{31})$. Figure 2 shows the imaginary part, $\mathrm{Im}(K)$, and the real part, $\mathrm{Re}(K)$, of $K(\omega)$. The solid blue lines are for the case of the SP; for comparison, the corresponding result for free space (i.e., the metamaterial-dielectric interface is absent) is also given by the dashed red lines. Parameters used for plotting the figure are $\kappa_{14} = 3 \times 10^{10}$ cm^{-1} s^{-1}, $\Omega_{c1(c2)} = 2\pi \times 19$ MHz, $\Delta_{2(3)} = -2\pi \times 1.6$ MHz, $\Delta_4 = -2\pi \times 31.8$ MHz, $\gamma_{41} = 2\pi \times 3.0$ MHz, $\gamma_{21} = 2\pi \times 1.6$ kHz, and $\gamma_{31} = 2\pi \times 1.6$ kHz. From Fig. 2(a) we see that there is an absorption minimum near $\omega = 0$ (corresponding to the center frequency of the probe field), and the height of the two side peaks is smaller than the case of the free space; from Fig. 2(b) one sees that, near $\omega = 0$, the slope of $\mathrm{Re}(K)$ is much bigger than the case of the free space, which means that the group velocity of the SP is much smaller than that in free space. These interesting characters are contributed by the quantum destructive interference effect of the EIT in the quantum emitters and by the mode confinement from the metamaterial-dielectric interface, which are very helpful to the realization of SP storage and splitting; see below.

The peak power P_{max} for generating the SP may be estimated by using Poyntings vector [48], which, based on

the system parameters given above, reads $P_{\max} \simeq 1.9$ nW. Consequently, to generate such SP only a very low input probe power is required, which is also due to the EIT effect and the mode-confinement effect in the system. This is in contrast with cases of nonresonant media [5–28], where much higher input power is needed for the formation of SPs.

B. SPBS without microwave field

We now turn to consider how to realize a SPBS in the system in the absence of the microwave fields. The method we propose here is that a single SP pulse is split into two in different times by employing the storage and retrieval of optical pulses [41] and SPs [44]. To this end, we assume that the two control fields are switched off and on successively, which can be modeled by the combination of two hyperbolic tangent functions with the form

$$\Omega_{c1}=\frac{1}{2}\Omega_{c10}\left[1-\sum_{i=1}^{2}\tanh\left(\frac{t-T^1_{\mathrm{off}_i}}{T_s}\right)+\tanh\left(\frac{t-T^1_{\mathrm{on}_1}}{T_s}\right)\right],$$
$$\Omega_{c2}=\Omega_{c20}\left[1-\frac{1}{2}\tanh\left(\frac{t-T^2_{\mathrm{off}_1}}{T_s}\right)+\frac{1}{2}\tanh\left(\frac{t-T^2_{\mathrm{on}_1}}{T_s}\right)\right], \quad (6)$$

where Ω_{cj0} $(j=1,2)$ are constants, T_s is switching time, and $T^j_{\mathrm{off}_i}$ ($T^j_{\mathrm{on}_i}$) is the ith switching off (switching on) of the control field Ω_{cj}. The timing sequences of the switching off and on of Ω_{cj} for obtaining a SPBS are illustrated in Fig. 3(a), with $T^1_{\mathrm{off}_1}=T^2_{\mathrm{off}_1}<T^1_{\mathrm{on}_1}<T^1_{\mathrm{off}_2}<T^2_{\mathrm{on}_1}$. In the figure, Ω_{c1} is plotted in the upper part by a solid red curve and Ω_{c2} is plotted in the lower part by a solid orange curve. The solid blue curves in the upper and lower parts are ones of the SP pulse Ω_p during its storage (when Ω_{c1} and Ω_{c2} are switched off) and splitting (when Ω_{c1} and Ω_{c2} are switched on successively) at position $x=3.25$ mm.

Shown in Fig. 3(c) is the result of a numerical simulation to obtain the SPBS by taking $|\Omega_p\tau_0|$ as a function of x and t/τ_0 (with $\tau_0=5.0\times10^{-8}$ s). In the simulation, the system parameters chosen are $\Delta_4=-2\pi\times31.8$ MHz, $\Delta_2=\Delta_3=-2\pi\times1.6$ MHz, $\gamma_{21}=2\pi\times1.6$ kHz, $\gamma_{31}=2\pi\times1.6$ kHz, $\gamma_{41}=2\pi\times2.7$ MHz, $\Omega_{c10}=\Omega_{c20}=2\pi\times48.9$ MHz, and $T_s=0.2\tau_0$. Several steps of the SP splitting can be described in the following.

(1) A single, weak linear probe pulse is incident at $x=0$ with waveform $\Omega_p(0,t)\tau_0=1.15e^{-t^2/\tau_0^2}$, and it is converted into a SP pulse by coupling with the metamaterial-dielectric interface. The SP pulse propagates forward with a larger dispersion and some Ohmic loss, and hence a change in shape during propagation is observed. The SP pulse obtained here is the one before storage; its distribution is illustrated by curves with red color (i.e., the part on the leftmost side of the figure).

(2) Both Ω_{c1} and Ω_{c2} are switched off at $t=T^1_{\mathrm{off}_1}=T^2_{\mathrm{off}_1}=7\tau_0$. The SP pulse is stored into the coherence $\tilde{\sigma}_{21}$, and also into the coherence $\tilde{\sigma}_{31}$ simultaneously. Figure 3(b) shows $\tilde{\sigma}_{21}$ and $\tilde{\sigma}_{31}$ as functions of x, at time $t=7\tau_0$ (solid red line) and $t=27\tau_0$ (dotted blue line) for $\tilde{\sigma}_{21}$, and $t=7\tau_0$ (solid red line) and $t=97\tau_0$ (dotted black line) for $\tilde{\sigma}_{31}$.

(3) By switching on Ω_{c1} at $t=T^1_{\mathrm{on}_1}=27\tau_0$ but keeping Ω_{c2} switched off, the emitter coherence $\tilde{\sigma}_{21}$ is converted back into the SP pulse, and hence a new SP pulse (called pulse 1) is retrieved. The middle blue pulses in the figure illustrate the propagation of the retrieved SP pulse to $x=4.2$, 5.6, and 7.0 mm (corresponding times are $t=31.9\tau_0$, $35.1\tau_0$, and $39.8\tau_0$), respectively.

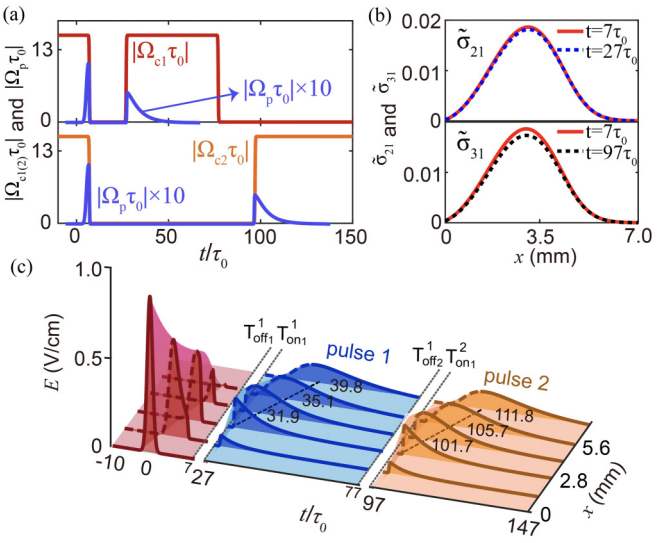

FIG. 3. SPBS realized by using two optical channels. (a) Timing sequences of the switching off and on of the two control fields Ω_{c1} (the solid red line in the upper part) and Ω_{c2} (the solid orange line in the lower part) for obtaining the SP splitting. The solid blue lines are curves of the SP pulse Ω_p during its storage (when Ω_{c1} and Ω_{c2} are switched off) and splitting (when Ω_{c1} and Ω_{c2} are switched on successively) at position $x=3.25$ mm. (b) Coherences of the quantum emitters as functions of distance x, at time $t=7\tau_0$ (solid red line) and $t=27\tau_0$ (dotted blue line) for $\tilde{\sigma}_{21}$, and $t=7\tau_0$ (solid red line) and $t=97\tau_0$ (dotted black line) for $\tilde{\sigma}_{31}$. (c) Electric field of the SP pulse as a function of x and t during the splitting process (i.e., propagation, storage, and retrieval) of the SP. For details, see text.

(4) At $t=T^1_{\mathrm{off}_2}=77\tau_0$, Ω_{c1} is switched off; after time $20\tau_0$, Ω_{c2} is switched on at $t=T^2_{\mathrm{on}_1}=97\tau_0$. The emitter coherence $\tilde{\sigma}_{31}$ is converted back into the SP pulse, and thus another new SP pulse (pulse 2) is retrieved. The rightmost orange pulses in the figure illustrate the propagation of the retrieved SP pulse to $x=4.2$, 5.6, and 7.0 mm (corresponding times are $t=101.7\tau_0$, $105.7\tau_0$, and $111.8\tau_0$), respectively.

From the figure, we see that the input probe pulse can be stored and retrieved through the switching off and on of the two control fields subsequently, thereby giving rise to the realization of the temporal splitting of the SP pulse, i.e., a SPBS. However, the retrieved SPs (i.e., pulse 1 and pulse 2) have smaller amplitudes compared with the input one. Approximated expressions of the probe pulse before and after storage are presented in Appendix B.

The quality of the SP splitting can be characterized by using the SP memory efficiency $\eta=1-\eta'$, with

$$\eta'=\frac{\left|\int_{-\infty}^{+\infty}dt\int_{-\infty}^{+\infty}dz\left|\mathbf{E}_p^{\mathrm{in}}\right|^2-\int_{-\infty}^{+\infty}dt\int_{-\infty}^{+\infty}dz\left|\mathbf{E}_p^{\mathrm{out}}\right|^2\right|}{\int_{-\infty}^{+\infty}dt\int_{-\infty}^{+\infty}dz\left|\mathbf{E}_p^{\mathrm{in}}\right|^2}, \quad (7)$$

where $\mathbf{E}_p^{\rm in} = \mathbf{E}_p^{\rm in}(0, z, t)$ (the input pulse) and $\mathbf{E}_p^{\rm out} = \mathbf{E}_p^{\rm out}(L_x, z, t)$ (the output pulse). From Fig. 3(c) and Eq. (7) we obtain $\eta = 34\%$ for $L_x = 7.0$ mm. The reasons for the low splitting efficiency here are the dephasing and dispersion of the quantum emitters and the residual Ohmic loss of the metamaterial.

C. SPBS with microwave fields

To improve the splitting efficiency of the SPBS, we can apply the two microwave fields to the quantum emitters [see Fig. 1(b)] in a suitable way. The Hamiltonian of the system in the presence of the microwave fields has been given in Appendix A.

The microwave fields Ω_{M1} and Ω_{M2} are taken to be continuous waves and do not couple to the SP mode [49]. The switching on and off of the microwave field can be modeled by

$$\Omega_{M_j}(x, t) = \frac{1}{2}\Omega_{M_j}(x)\left[\tanh\left(\frac{t - T_{\rm off}^{M_j}}{T_s}\right) - \tanh\left(\frac{t - T_{\rm on}^{M_j}}{T_s}\right)\right], \tag{8}$$

where T_s is the same as used in Eq. (6) and $T_{\rm off}^{M_j}$ ($T_{\rm on}^{M_j}$) is the time of switching off (switching on) of the microwave field Ω_{M_j}. We take $T_{\rm on}^{M1} > T_{\rm off_1}^1$, $T_{\rm off}^{M1} < T_{\rm on_1}^1$, $T_{\rm on}^{M2} > T_{\rm off_2}^1$, and $T_{\rm off}^{M2} < T_{\rm on_1}^2$, which means that the microwave fields play roles only within the time interval of the respective storage periods. In addition, amplitudes of the microwave fields are taken to be functions of x, also aiming to obtain high splitting efficiency of the SP. Based on these considerations, we assume the amplitudes of the microwave fields have the form $\Omega_{M1(M2)}(x) = \Omega_{M10(M20)} \exp\{-[(x - a_{1(2)})/b_{1(2)}]^2\}$, where $\Omega_{M10(M20)}$ are the maximum of the amplitudes and $a_{1(2)}$ and $b_{1(2)}$ are two arbitrary parameters, which can be chosen to optimize the splitting efficiency.

The timing sequences of the switching off and on of the control fields Ω_{c1} and Ω_{c2} for obtaining the SPBS are illustrated in Fig. 4(a), which are similar to Fig. 3(a), but with new timing sequence curves of the microwave fields Ω_{M1} (the solid green line in the upper part) and Ω_{M2} (the solid purple line in the lower part) added. The inset gives the spatial shape of the microwave fields [$\Omega_{M1}(x) = \Omega_{M2}(x)$ is assumed]. The solid blue lines in the figure have the same meaning indicated in Fig. 3(a). When plotting the figure, we have taken $\Omega_{M10}\tau_0 = \Omega_{M20}\tau_0 = 0.0025$ (i.e., $\Omega_{M10} = \Omega_{M20} = 2\pi \times 7.96$ kHz); other parameters are the same as those used above.

Figure 4(b) shows the coherences of the quantum emitters, i.e., $\tilde{\sigma}_{21}$ and $\tilde{\sigma}_{31}$, during the storage periods as functions of $t = 7\tau_0$ (solid red line) and $t = 27\tau_0$ (dotted blue line) for $\tilde{\sigma}_{21}$, and $t = 7\tau_0$ (solid red line) and $t = 97\tau_0$ (dotted black line) for $\tilde{\sigma}_{31}$. One sees that compared with the case without the use of the microwave fields given in Fig. 3(b), the coherences are increased significantly.

Illustrated in Fig. 4(c) is the electric field of the SP pulse as a function of x and t during the propagation, storage, and splitting. Shown on the leftmost side of the figure is the space-time distribution of the SP pulse before the storage, represented by solid red curves. The middle part is the space-time

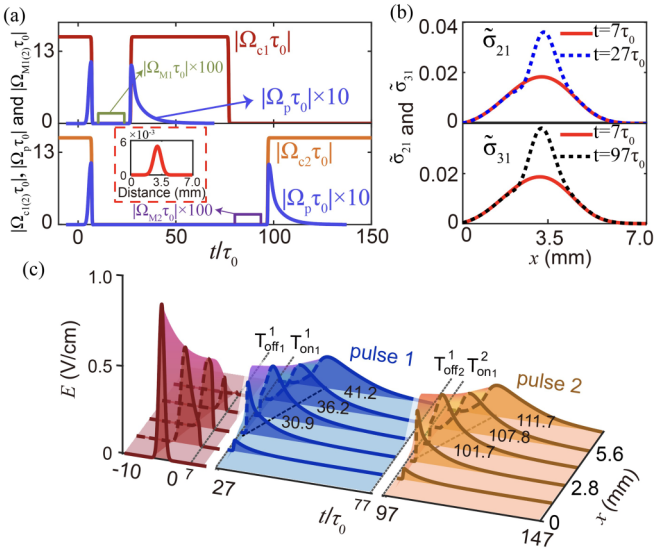

FIG. 4. SPBS realized by using two optical channels with the use of two microwave fields. (a) Similar to Fig. 3(a) but with the timing sequences of the microwave field Ω_{M1} (the solid green line in the upper part) and Ω_{M2} (the solid purple line in the lower part) shown. Inset: the spatial shape of the microwave fields [$\Omega_{M1}(x) = \Omega_{M2}(x)$ is assumed]. Solid blue lines: similar to those indicated in Fig. 3(a). (b) Coherences of the quantum emitters as a function of distance x at time $t = 7\tau_0$ (solid red line) and $t = 27\tau_0$ (dotted blue line) for $\tilde{\sigma}_{21}$, and $t = 7\tau_0$ (solid red line) and $t = 97\tau_0$ (dotted black line) for $\tilde{\sigma}_{31}$. (c) Electric field for SP pulse as a function of x and t during the splitting process (i.e., propagation, storage, and retrieval) of the SP. For details, see text.

distribution of the first split (retrieved) SP pulse, represented by solid blue curves with corresponding propagating times respectively at $t = 30.9\tau_0$, $36.2\tau_0$, and $41.1\tau_0$. Curves for the space-time distribution of the second split (retrieved) SP pulse are plotted on the rightmost part of the figure, where the solid orange curves correspond to the propagating times at $t = 101.7\tau_0$, $107.8\tau_0$, and $111.7\tau_0$, respectively. We see that, compared to the case without the microwave fields, the amplitudes (widths) of the split SP pulses are larger (smaller) than those without the microwave fields. By the formula (7), we can estimate the splitting efficiency of the SP in the presence of the microwave fields, given by $\eta = 84\%$, much higher than that without the use of the microwave fields. A detailed analysis for understanding the improvement of the splitting efficiency with the use of the microwave fields has been presented in Appendix B.

D. Surface polaritonic soliton beam splitters

Although the use of the microwave fields can improve the splitting efficiency, the SP pulse still experiences dispersion, resulting in the lowering of the pulse amplitude and the broadening of the pulse width [which can be seen clearly for split SP pulses given in Figs. 3(c) and 4(c)], and hence lowers the splitting efficiency. To solve this problem, here we prove that the EIT-enhanced Kerr nonlinearity in the system can be employed to balance the dispersion so as to improve the SP splitting efficiency further.

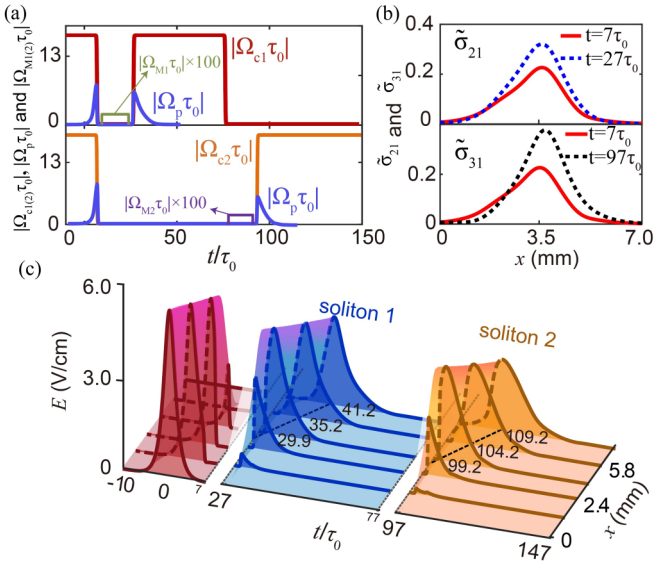

FIG. 5. Surface polaritonic soliton beam splitters through two optical channels. (a) Timing sequences of the control fields and microwave fields [similar to Fig. 4(a)]. The solid blue lines are curves of the soliton pulse Ω_p during the storage (when Ω_{c1} and Ω_{c2} are switched off) and splitting (when Ω_{c1} and Ω_{c2} are switched on successively) at position $x = 3.50$ mm. (b) Coherences of the quantum emitters as functions of distance x at time $t = 7\tau_0$ (red solid line) and $t = 27\tau_0$ (blue dotted line) for $\tilde{\sigma}_{21}$, and $t = 7\tau_0$ (red solid line) and $t = 97\tau_0$ (black dotted line) for $\tilde{\sigma}_{31}$. (c) The electric field of the surface polaritonic soliton as a function of x and t during the splitting process (i.e., propagation, storage, and retrieval) of the SP. For details, see text.

We first show that the system supports surface polaritonic solitons. By using the method of multiple scales [48], we can derive, from the MB Eqs. (3) and (4), a nonlinear equation describing the evolution of the envelope F of the SP, with the form $i\frac{\partial}{\partial x}F - \frac{1}{2}K_2\frac{\partial^2}{\partial\tau^2}F + W|F|^2F\,e^{-2\alpha z} = 0$, where $\tau = t - x/V_g$, $V_g \equiv (\partial K/\partial\omega)^{-1}$ (group velocity), and $\alpha = \mathrm{Im}(K)$ (absorption coefficient). The coefficients W and $K_2 = \partial^2 K/\partial\omega^2$ describe self-phase modulation (Kerr nonlinearity) and group-velocity dispersion, respectively. The detailed derivation of this nonlinear envelope equation has been presented in Appendix C.

The third-order nonlinear optical susceptibility of the system, $\chi_p^{(3)}$, is proportional to the self-phase modulation coefficient W via the relation $\chi_p^{(3)} = \frac{2c}{\omega_p}\frac{|\mathbf{p}_{14}|^2}{\hbar^2}W$. Based on the system parameters we obtain $\chi_p^{(3)} = 3.6\times10^{-2}\ \mathrm{cm^2\,V^{-2}}$ (small imaginary is neglected). Such large Kerr nonlinearity comes from the EIT enhancement and the light confinement near the metamaterail-dielectric interface. Because, due to the EIT effect, α and the imaginary parts of W and K_2 are small, the nonlinear envelope equation admits the approximate soliton solution $\Omega_p(x,t) = \frac{1}{\tau_0}\sqrt{\frac{|K_2|}{W}}\mathrm{sech}[\frac{1}{\tau_0}(t - \frac{x}{V_g})]\,e^{i[K-1/(2L_D)]x}$, where $L_D \equiv \tau_0^2/|K_2|$ is the dispersion length of the system.

The surface polaritonic soliton splitter is obtained by the storage and retrieval of the soliton. Illustrated in Fig. 5(a) are the timing sequences of the two control fields and the two microwave fields, which are similar to those used in Fig. 4(a). The solid blue lines are curves of the soliton pulse Ω_p during its storage (when Ω_{c1} and Ω_{c2} are switched off) and splitting (when Ω_{c1} and Ω_{c2} are switched on successively) at position $x = 3.50$ mm. Figure 5(b) shows the coherences $\tilde{\sigma}_{21}$ and $\tilde{\sigma}_{31}$ of the system. One sees that, in the soliton case, the coherences are much higher than the linear cases [Fig. 3(b) and Fig. 4(b)].

Shown in Fig. 5(c) is the result of a numerical simulation on the soliton splitting by taking $|\Omega_p\tau_0|$ as a function of t/τ_0 and x (with $\tau_0 = 5.0\times10^{-8}$ s), i.e., $\Omega_p\tau_0 = 8.5\,\mathrm{sech}(t/1.6\tau_0)$. We see that, due to the balance between the group-velocity dispersion and the Kerr nonlinearity, widths (amplitudes) of the two split solitons are smaller (higher) than those in the linear cases [Figs. 3(c) and 4(c)]. Using the formula (7), we obtain the splitting efficiency of the soliton beam splitter, given by $\eta = 95\%$, which is higher than those obtained by using the linear SPs discussed above. A discussion on the solitonic character of the split nonlinear SPs and the difference between the two split SPs shown in Fig. 5(c) has been given in Appendix D.

For practical applications, it is desirable to make the system work at a room temperature. In this situation, the inhomogeneous line broadening of the quantum emitters is usually not negligible, which may degrade the property of EIT [50] and hence the behavior of the SPBS. To show this, here we take a realistic example by choosing Pr:YSO as the dielectric of the metamaterial-dielectric interface, where Pr^{3+} ions are doped into the Pr:YSO layer near the interface. A numerical simulation is carried out for a surface polaritonic soliton beam splitting by assuming, for simplicity, that the inhomogeneous line broadening is represented by modified parameters of the spontaneous emission and dephasing, i.e., $\Gamma_4 = 2\pi\times0.16$ GHz and $\gamma_{21} = \gamma_{32} = \gamma_{32} = 2\pi\times1.59$ kHz [50], with the other parameters the same as those used above. The result shows that, due to the influence of the inhomogeneous broadening, the decay of the soliton is faster than that without the inhomogeneous broadening, which makes the soliton splitting efficiency reduce into $\eta = 64\%$ (for detail, see Appendix E). Although the splitting efficiency is lowered, it is still high and hence may be applicable at room-temperature environment.

E. Surface polariton router

An all-optical router is a device for sending or routing an incident optical signal into one or several output channels, which is very useful for the realization of all-optical network [51]. For practical applications, compact solid surface polariton routers (SPRs) for optical and quantum information processing are desirable components for photonic networks on chips [52].

As an extension of the SPBS, here we show that a SPR can be realized by exploiting the dielectric-metamaterial interface doped with quantum emitters [Fig. 1(a)]. The basic principle of the SPR is the following: after stored and retrieved in the dielectric-metamaterial interface, the input probe pulse is split and routed onto several optical pulses with different frequencies and/or powers by manipulating two or more control fields simultaneously.

For simplicity, we consider a scheme for realizing a SPR with only two output optical channels. In this case, the quantum emitters are assumed to have an excitation scheme with

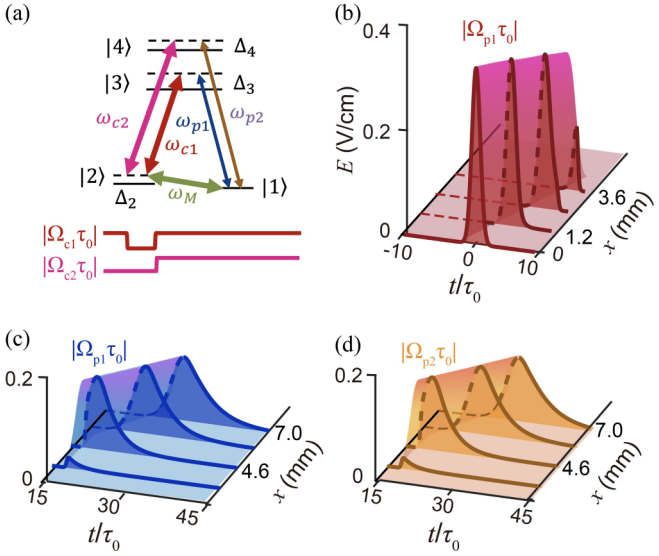

FIG. 6. Surface polariton router (SPR) realized in the quantum emitter-doped dielectric-metamaterial interface with two output optical channels. (a) Excitation scheme of the quantum emitters with a double-Λ-type level configuration. For more detail, see text. (b) The input SP pulse $|\Omega_{p1}\tau_0|$ as a function of propagation distance x and time t before storage. (c),(d) Two SP pulses (i.e., $|\Omega_{p1}\tau_0|$ and $|\Omega_{p2}\tau_0|$) with different frequencies and powers are obtained by splitting the input PS pulse through the use of two control fields Ω_{c1} and Ω_{c2} simultaneously.

a double-Λ-type level configuration [see Fig. 6(a)]. To realize the SPR, the two control fields (with angular frequencies ω_{c1}, ω_{c2} and half Rabi frequencies Ω_{c1}, Ω_{c2}, respectively) and a microwave field (with angular frequency ω_M and half Rabi frequency Ω_M) in the system must be switched off and on in a suitable way.

First, by switching on the control field Ω_{c1}, the input SP field Ω_{p1} propagates in the system, as shown in Fig. 6(b) as a function of propagation distance x and time t. Second, by switching off Ω_{c1}, the SP field Ω_{p1} is stored in the quantum emitters. Then, during the storage period the microwave field is applied, which can provide a gain to the stored SP field. Third, by turning off the microwave field and switching on the two control fields Ω_{c1} and Ω_{c2} simultaneously, two SP pulses (i.e., Ω_{p1} and Ω_{p2}) are retrieved [see Fig. 6(c) and Fig. 6(d)]. Since these two retrieved SP pulses are obtained by the splitting of the stored PS pulse, they have different frequencies and powers. In this way, the system behaves as a SPR with two output optical channels. Obviously, one can also realize a SPR with more output optical channels by using more control fields in the retrieval process of the SP pulse.

IV. SUMMARY

As shown above, the scheme for realizing the SPBS using the quantum hybrid system can have a high splitting efficiency. We stress that such a scheme can also be manipulated actively in a controllable way. For instance, one can obtain different SPBS by selecting different quantum emitters and their level structures, by turning the amplitudes and time sequences of the switching off and switching on of the two control fields, and so on. Moreover, it can be extended to cases with more optical channels by using more control fields, and hence the two-channel splitting SPBS shown in the last section can be generalized to multiple channel ones. In Appendix F, we have presented an example of three-channel SPBS, realized with the same metamaterial-dielectric interface, but with the quantum emitters having a quadripod type level configuration interacting with three control fields.

In conclusion, in this work we have proposed a scheme for realizing highly efficient and controllable SPBS with a hybrid quantum system via EIT of the quantum emitters that are doped near a metamaterial dielectric. By virtue of the destructive interference effects contributed by the EIT of the quantum emitters and by the joint electric and magnetic responses of the metamaterial, we have shown that such beam splitters can work with very low light power [53] and they have small quantum decoherence and low Ohmic loss. Moreover, we have demonstrated that the propagation loss of the SPs can be reduced further by using weak microwave fields and the dispersion effect of the SPs can be canceled by using the EIT-enhanced Kerr effect. As a result, the SPBS obtained not only have high splitting efficiency but also can be manipulated and controlled actively. Our research opens a way for coherent and active control of low-loss SPs and for promising applications in optical information processing and transmission based on solid quantum hybrid systems.

ACKNOWLEDGMENTS

The authors thank C. Hang, J. Su, D. Xu, and Q. Zhang for useful discussions. This work was supported by the National Natural Science Foundation of China under Grants No. 11474099 and No. 19975098.

APPENDIX A: MB EQUATIONS

Under rotating-wave approximation, in the interaction picture the Hamiltonian of the system in the presence of the two microwave fields reads

$$\hat{H}_{\rm int}=-\hbar\Bigg[\sum_{j=1}^{4}\Delta_j|j\rangle\langle j|+(\zeta_p(z)\Omega_p|4\rangle\langle 1|+\zeta_{c1}(z)\Omega_{c1}|4\rangle\langle 2| +\zeta_{c2}(z)\Omega_{c2}|4\rangle\langle 3|+\Omega_{M1}|2\rangle\langle 1|+\Omega_{M2}|3\rangle\langle 1|+\text{H.c.})\Bigg], \tag{A1}$$

where $\Delta_1=0$, $\Delta_4=\omega_p-(E_4-E_1)/\hbar$ (one-photon detuning), $\Delta_2=\omega_p-\omega_{c1}-(E_2-E_1)/\hbar$, and $\Delta_3=\omega_p-\omega_{c2}-(E_3-E_1)/\hbar$ (two-photon detunings); E_j $(j=1,\ 2,\ 3,\ 4)$ is the energy eigenvalue of the quantum emitters at eigenstate $|j\rangle$; $\Omega_p(\mathbf{r},t)=\xi_p(\mathbf{r},t)|\mathbf{p}_{41}|/\hbar$, $\Omega_{c1(c2)}=\xi_{c1(c2)}|\mathbf{p}_{42(43)}|/\hbar$, and $\Omega_{M1(M2)}=E_{M1(M2)}|\mathbf{p}_{21(31)}|/\hbar$ are, respectively, half Rabi frequencies of the probe, control, and microwave fields, with $\mathbf{p}_{jl}$ the electric dipole matrix element associated with the transition from state $|j\rangle$ and state $|l\rangle$.

Explicit expressions of the equations of motion of the density-matrix elements σ_{jl} describing the evolution of the quantum emitters (i.e., the optical Bloch equations) read

$$i\frac{\partial}{\partial t}\sigma_{11} - i\Gamma_{14}\sigma_{44} + \zeta(z)\Omega_p^*\sigma_{41} - \zeta(z)\Omega_p\sigma_{41}^* + \Omega_{M1}^*\sigma_{21} - \Omega_{M1}\sigma_{21}^* + \Omega_{M2}^*\sigma_{31} - \Omega_{M2}\sigma_{31}^* = 0, \tag{A2a}$$

$$i\frac{\partial}{\partial t}\sigma_{22} - i\Gamma_{24}\sigma_{44} + \zeta(z)\Omega_{c1}^*\sigma_{42} - \zeta(z)\Omega_{c1}\sigma_{42}^* + \Omega_{M1}\sigma_{21}^* - \Omega_{M1}^*\sigma_{21} = 0, \tag{A2b}$$

$$i\frac{\partial}{\partial t}\sigma_{33} - i\Gamma_{34}\sigma_{44} + \zeta(z)\Omega_{c2}^*\sigma_{43} - \zeta(z)\Omega_{c2}\sigma_{43}^* + \Omega_{M2}\sigma_{31}^* - \Omega_{M2}^*\sigma_{31} = 0, \tag{A2c}$$

$$i\frac{\partial}{\partial t}\sigma_{44} + i\Gamma_4\sigma_{44} - \zeta(z)\Omega_p^*\sigma_{41} + \zeta(z)\Omega_p\sigma_{41}^* - \zeta(z)\Omega_{c1}^*\sigma_{42} + \zeta(z)\Omega_{c1}\sigma_{42}^* - \zeta(z)\Omega_{c2}^*\sigma_{43} + \zeta(z)\Omega_{c2}\sigma_{43}^* = 0, \tag{A2d}$$

$$\left(i\frac{\partial}{\partial t} + d_{21}\right)\sigma_{21} - \zeta(z)\Omega_p\sigma_{42}^* + \zeta(z)\Omega_{c1}^*\sigma_{41} + \Omega_{M1}(\sigma_{11} - \sigma_{22}) - \Omega_{M2}\sigma_{32}^* = 0, \tag{A2e}$$

$$\left(i\frac{\partial}{\partial t} + d_{31}\right)\sigma_{31} - \zeta(z)\Omega_p\sigma_{43}^* + \zeta(z)\Omega_{c2}^*\sigma_{41} + \Omega_{M2}(\sigma_{11} - \sigma_{33}) - \Omega_{M1}\sigma_{32} = 0, \tag{A2f}$$

$$\left(i\frac{\partial}{\partial t} + d_{32}\right)\sigma_{32} - \zeta(z)\Omega_{c1}\sigma_{43}^* + \zeta(z)\Omega_{c2}^*\sigma_{42} + \Omega_{M2}\sigma_{21}^* - \Omega_{M1}^*\sigma_{31} = 0, \tag{A2g}$$

$$\left(i\frac{\partial}{\partial t} + d_{41}\right)\sigma_{41} - \zeta(z)\Omega_p(\sigma_{44} - \sigma_{11}) + \zeta(z)\Omega_{c1}\sigma_{21} + \zeta(z)\Omega_{c2}\sigma_{31} - \Omega_{M1}\sigma_{42} - \Omega_{M2}\sigma_{43} = 0, \tag{A2h}$$

$$\left(i\frac{\partial}{\partial t} + d_{42}\right)\sigma_{42} - \zeta(z)\Omega_{c1}(\sigma_{44} - \sigma_{22}) + \Omega_p\sigma_{21}^* + \zeta(z)\Omega_{c2}\sigma_{32} - \Omega_{M1}^*\sigma_{41} = 0, \tag{A2i}$$

$$\left(i\frac{\partial}{\partial t} + d_{43}\right)\sigma_{43} - \zeta(z)\Omega_{c2}(\sigma_{44} - \sigma_{33}) + \Omega_p\sigma_{31}^* + \zeta(z)\Omega_{c1}\sigma_{32}^* - \Omega_{M2}^*\sigma_{41} = 0, \tag{A2j}$$

with $d_{jl} = \Delta_j - \Delta_l + i\gamma_{jl}$, where $\gamma_{jl} = (\Gamma_j + \Gamma_l)/2 + \gamma_{jl}^{\rm dep}$ is the decay rate of the emitter coherence σ_{jl}, $\Gamma_j = \sum_{E_l<E_j}\Gamma_{lj}$ is the spontaneous-emission rate of the state $|j\rangle$, and $\gamma_{jl}^{\rm dep}$ is the dephasing rate representing the loss of phase coherence between $|j\rangle$ and $|l\rangle$ contributed by the incoherent processes in the emitters.

Since the mode function $\zeta(z)$ that provides the confinement of the electric field in the vertical direction is a fast varying function of z, the Bloch Eqs. (A2) can be simplified by defining [43] $\tilde{\sigma}_{jj}(x,t) = \int_{-\infty}^{+\infty} dz|\zeta(z)|^2\sigma_{jj}(x,z,t)/\int_{-\infty}^{+\infty} dz|\zeta(z)|^2$ ($j = 1, 2, 3, 4$), $\tilde{\sigma}_{31(32,21)}(x,t) = \int_{-\infty}^{+\infty} dz|\zeta(z)|^2\sigma_{31(32,21)}(x,z,t)$, and $\tilde{\sigma}_{41(42,43)}(x,t)\zeta(z) = \sigma_{41(42,43)}(x,z,t)$. Then we get the reduced the Bloch equations

$$i\frac{\partial}{\partial t}\tilde{\sigma}_{11} - i\Gamma_{14}\tilde{\sigma}_{44} + \rho\Omega_p^*\tilde{\sigma}_{41} - \rho\Omega_p\tilde{\sigma}_{41}^* + \Omega_{M1}^*\tilde{\sigma}_{21} - \Omega_{M1}\tilde{\sigma}_{21}^* + \Omega_{M2}^*\tilde{\sigma}_{31} - \Omega_{M2}\tilde{\sigma}_{31}^* = 0, \tag{A3a}$$

$$i\frac{\partial}{\partial t}\tilde{\sigma}_{22} - i\Gamma_{24}\tilde{\sigma}_{44} + \rho\Omega_{c1}^*\tilde{\sigma}_{42} - \rho\Omega_{c1}\tilde{\sigma}_{42}^* + \Omega_{M1}\tilde{\sigma}_{21}^* - \Omega_{M1}^*\tilde{\sigma}_{21} = 0, \tag{A3b}$$

$$i\frac{\partial}{\partial t}\tilde{\sigma}_{33} - i\Gamma_{34}\tilde{\sigma}_{44} + \rho\Omega_{c2}^*\tilde{\sigma}_{43} - \rho\Omega_{c2}\tilde{\sigma}_{43}^* + \Omega_{M2}\tilde{\sigma}_{31}^* - \Omega_{M2}^*\tilde{\sigma}_{31} = 0, \tag{A3c}$$

$$i\frac{\partial}{\partial t}\tilde{\sigma}_{44} + i\Gamma_4\tilde{\sigma}_{44} - \rho\Omega_p^*\tilde{\sigma}_{41} + \rho\Omega_p\tilde{\sigma}_{41}^* - \rho\Omega_{c1}^*\tilde{\sigma}_{42} + \rho\Omega_{c1}\tilde{\sigma}_{42}^* - \rho\Omega_{c2}^*\tilde{\sigma}_{43} + \rho\Omega_{c2}\tilde{\sigma}_{43}^* = 0, \tag{A3d}$$

$$\left(i\frac{\partial}{\partial t} + d_{21}\right)\tilde{\sigma}_{21} - \rho\Omega_p\tilde{\sigma}_{42}^* + \rho\Omega_{c1}^*\tilde{\sigma}_{41} + \Omega_{M1}(\tilde{\sigma}_{11} - \tilde{\sigma}_{22}) - \Omega_{M2}\tilde{\sigma}_{32}^* = 0, \tag{A3e}$$

$$\left(i\frac{\partial}{\partial t} + d_{31}\right)\tilde{\sigma}_{31} - \rho\Omega_p\tilde{\sigma}_{43}^* + \rho\Omega_{c2}^*\tilde{\sigma}_{41} + \Omega_{M2}(\tilde{\sigma}_{11} - \tilde{\sigma}_{33}) - \Omega_{M1}\tilde{\sigma}_{32} = 0, \tag{A3f}$$

$$\left(i\frac{\partial}{\partial t} + d_{32}\right)\tilde{\sigma}_{32} - \rho\Omega_{c1}\tilde{\sigma}_{43}^* + \rho\Omega_{c2}^*\tilde{\sigma}_{42} + \Omega_{M2}\tilde{\sigma}_{21}^* - \Omega_{M1}^*\tilde{\sigma}_{31} = 0, \tag{A3g}$$

$$\left(i\frac{\partial}{\partial t} + d_{41}\right)\tilde{\sigma}_{41} - \rho\Omega_p(\tilde{\sigma}_{44} - \tilde{\sigma}_{11}) + \rho\Omega_{c1}\tilde{\sigma}_{21} + \rho\Omega_{c2}\tilde{\sigma}_{31} - \Omega_{M1}\tilde{\sigma}_{42} - \Omega_{M2}\tilde{\sigma}_{43} = 0, \tag{A3h}$$

$$\left(i\frac{\partial}{\partial t} + d_{42}\right)\tilde{\sigma}_{42} - \rho\Omega_{c1}(\tilde{\sigma}_{44} - \tilde{\sigma}_{22}) + \rho\Omega_p\tilde{\sigma}_{21}^* + \rho\Omega_{c2}\tilde{\sigma}_{32} - \Omega_{M1}^*\tilde{\sigma}_{41} = 0, \tag{A3i}$$

$$\left(i\frac{\partial}{\partial t} + d_{43}\right)\tilde{\sigma}_{43} - \rho\Omega_{c2}(\tilde{\sigma}_{44} - \tilde{\sigma}_{33}) + \rho\Omega_p\tilde{\sigma}_{31}^* + \rho\Omega_{c1}\tilde{\sigma}_{32}^* - \Omega_{M2}^*\tilde{\sigma}_{41} = 0, \tag{A3j}$$

where $\rho = \int_{-\infty}^{+\infty} dz|\zeta(z)|^4 / \int_{-\infty}^{+\infty} dz|\zeta(z)|^2$ is a parameter describing the mode confinement of the metamaterial-dielectric interface in the z direction.

The evolution of the probe field is described by the Maxwell equation $\nabla^2\mathbf{E} - (1/c^2)\partial^2\mathbf{E}/\partial t^2 = (1/\varepsilon_0 c^2)\partial^2\mathbf{P}/\partial t^2$, with the electric polarization intensity given by

$$\begin{aligned}\mathbf{P}(\mathbf{r},t) = \mathcal{N}_{\mathrm{QE}}(z)(&\mathbf{p}_{14}\sigma_{41}e^{i(k_p x-\omega_p t)} + \mathbf{p}_{24}\sigma_{42}e^{i(k_{c1}x-\omega_{c1}t)} \\ &+ \mathbf{p}_{34}\sigma_{43}e^{i(k_{c2}x-\omega_{c2}t)} + \mathbf{p}_{12}\sigma_{21}e^{i(k_{M1}x-\omega_{M1}t)} \\ &+ \mathbf{p}_{13}\sigma_{31}e^{i(k_{M2}x-\omega_{M2}t)} + \mathrm{c.c.}),\end{aligned} \tag{A4}$$

where $\mathcal{N}_a(z)$ is the number density of the quantum emitters and $\mathbf{P}_{\mathrm{host}} = \varepsilon_0\chi_{\mathrm{host}}\mathbf{E}$ is the electric polarization intensity of the system in the absence of the quantum emitters, with χ_{host} the corresponding susceptibility, which is assumed to be linear for simplicity. Under slowly varying envelope approximation, the Maxwell equation is simplified into

$$i\left(\frac{\partial}{\partial x} + \frac{n_2^2}{n_{\mathrm{eff}}c}\frac{\partial}{\partial t}\right)\Omega_p + \langle\kappa_{14}(z)\tilde{\sigma}_{41}\rangle = 0, \tag{A5}$$

where n_2 is the refractive index of the dielectric and $\kappa_{14}(z) \equiv \mathcal{N}_{\mathrm{QE}}(z)|\mathbf{p}_{14}|^2\omega_p/(2n_{\mathrm{eff}}\hbar\varepsilon_0 c)$ with $n_{\mathrm{eff}} \equiv ck/\omega_p$ the effective refractive index of the system in the absence of the emitters.

APPENDIX B: ANALYSIS FOR IMPROVING THE SPBS QUALITY BY THE USE OF THE MICROWAVE FIELDS

To get a clear understanding on how the microwave fields can provide a gain to the SP and hence to suppress its loss during propagation and improve the SPBS quality, here we give an approximate solution of the SP by solving the Bloch Eq. (A2) when the microwave fields are present.

Note that before the storage of the SP, i.e., the two control fields are on and the microwave fields are not applied, $d_{31}\tilde{\sigma}_{31}$ ($d_{32}\tilde{\sigma}_{32}$) is small, and $\Omega_{M1(M2)}$ and $\tilde{\sigma}_{42}$ ($\tilde{\sigma}_{43}$) are zero. We have

$$\begin{aligned}\sigma_{41} = &-\frac{i}{|\zeta(z)\Omega_{c1}|^2 + |\zeta(z)\Omega_{c2}|^2} \\ &\times\left(\zeta(z)\Omega_{c1}\frac{\partial\sigma_{21}}{\partial t} + \zeta(z)\Omega_{c2}\frac{\partial\sigma_{31}}{\partial t}\right).\end{aligned} \tag{B1}$$

Substituting Eq. (B1) into Eq. (A2) and using $\sigma_{11} \approx 1$ and $\sigma_{44} \approx 0$, we obtain

$$\begin{aligned}&\zeta(z)\Omega_{c1}\sigma_{21} + \zeta(z)\Omega_{c2}\sigma_{31} \\ &= -\zeta(z)\Omega_p - \frac{1}{|\zeta(z)\Omega_{c1}|^2 + |\zeta(z)\Omega_{c2}|^2} \\ &\times\left(\frac{\partial}{\partial t} + id_{41}\right)\left[\zeta(z)\Omega_{c1}\frac{\partial\sigma_{21}}{\partial t} + \zeta(z)\Omega_{c2}\frac{\partial\sigma_{31}}{\partial t}\right] \\ &\simeq -\zeta(z)\Omega_p.\end{aligned} \tag{B2}$$

Equation (B2) can be rewritten as the form $\sigma_{21} + (\Omega_{c2}/\Omega_{c1})\sigma_{31} \simeq -(\Omega_p/\Omega_{c1})$. Therefore, σ_{21} and σ_{31} are nonzero if Ω_{c2}/Ω_{c1} and Ω_p/Ω_{c1} have finite values. During the storage period, though Ω_{c1} and Ω_{c2} approach zero, Ω_p also approaches zero, and hence σ_{21} and σ_{31} are still nonzero, i.e., the information of the SP in converted into the two coherences of the quantum emitters during the storage period.

In the retrieval (splitting) period, the SP pulse is recovered when Ω_{c1} and Ω_{c2} are switched on again. By solving Eq. (A2) we obtain

$$\begin{aligned}\tilde{\sigma}_{21}\left(x, T_{\mathrm{on}_1}^1\right) = &-\frac{\Omega_{c1}\Omega_p\left(x, T_{\mathrm{off}_1}^1\right)}{|\Omega_c|^2}e^{id_{21}\left(T_{\mathrm{on}_1}^1 - T_{\mathrm{off}_1}^1\right)} \\ &+ \frac{\Omega_{M1}(x)}{d_{21}}\left[e^{id_{21}\left(T_{\mathrm{on}}^{M1} - T_{\mathrm{off}}^{M1}\right)} - 1\right],\end{aligned} \tag{B3a}$$

$$\begin{aligned}\tilde{\sigma}_{31}\left(x, T_{\mathrm{on}_1}^2\right) = &-\frac{\Omega_{c2}\Omega_p\left(x, T_{\mathrm{off}_1}^1\right)}{|\Omega_c|^2}e^{id_{31}\left(T_{\mathrm{on}_1}^2 - T_{\mathrm{off}_1}^2\right)} \\ &+ \frac{\Omega_{M2}(x)}{d_{31}}\left[e^{id_{31}\left(T_{\mathrm{on}}^{M2} - T_{\mathrm{off}}^{M2}\right)} - 1\right],\end{aligned} \tag{B3b}$$

where $|\Omega_c|^2 = |\Omega_{c1}|^2 + |\Omega_{c2}|^2$. We see that the microwave fields Ω_{M1} and Ω_{M2} have contributions to the emitter coherences $\tilde{\sigma}_{21}$ and $\tilde{\sigma}_{31}$, which provide a gain to both SPs that are retrieved (split) successively in later times.

To see how the microwave fields can contribute gain to the probe field, we solve Eq. (A2) during the retrieval (splitting) period of the SP, with the result given by

$$\begin{aligned}\Omega_p^{\mathrm{out1}}\left(x, T_{\mathrm{on}_1}^1\right) = &\frac{|\Omega_{c1}|^2\Omega_p\left(x, T_{\mathrm{off}_1}^1\right)}{|\Omega_c|^2}e^{id_{21}\left(T_{\mathrm{on}_1}^1 - T_{\mathrm{off}_1}^1\right)} \\ &+ \frac{\Omega_{c1}\Omega_{M1}(x)}{d_{21}}\left[1 - e^{id_{21}\left(T_{\mathrm{on}}^{M1} - T_{\mathrm{off}}^{M1}\right)}\right],\end{aligned} \tag{B4a}$$

$$\begin{aligned}\Omega_p^{\mathrm{out2}}\left(x, T_{\mathrm{on}_1}^2\right) = &\frac{|\Omega_{c2}|^2\Omega_p\left(x, T_{\mathrm{off}_1}^1\right)}{|\Omega_c|^2}e^{id_{31}\left(T_{\mathrm{on}_1}^2 - T_{\mathrm{off}_1}^2\right)} \\ &+ \frac{\Omega_{c2}\Omega_{M2}(x)}{d_{31}}\left[1 - e^{id_{31}\left(T_{\mathrm{on}}^{M2} - T_{\mathrm{off}}^{M2}\right)}\right],\end{aligned} \tag{B4b}$$

where $\Omega_p^{\mathrm{out1}}(x, T_{\mathrm{on}_1}^1)$ is the first SP that is retrieved at time $T_{\mathrm{on}_1}^1$ and $\Omega_p^{\mathrm{out2}}(x, T_{\mathrm{on}_2}^1)$ is the second SP that is retrieved at time $T_{\mathrm{on}_2}^2$. Based on this result, we obtain explicit expressions of the retrieved (split) two SP pulses (for later time evolution)

$$\begin{aligned}\Omega_p^{\mathrm{out1}}(x,t') = &\frac{|\Omega_{c1}|^2\Omega_p(0,0)\exp(id_{21}t_1)}{|\Omega_c|^2\sqrt{1 - 2iK_2(x - t'/K_1')/\tau_0^2}}\exp\left\{iK_0(x - t'/K_1') - \frac{\left[K_1(x - t'/K_1') - T_{\mathrm{off}_1}^1\right]^2}{[1 - 2iK_2(x - t'/K_1')]/\tau_0^2}\right\} \\ &+ \frac{\Omega_{c1}\Omega_{M10}}{d_{21}}\left\{1 - \exp\left[id_{21}\left(T_{\mathrm{on}}^{M1} - T_{\mathrm{off}}^{M1}\right)\right]\right\}\exp\left[-\frac{(x - a_1 - t'/K_1')^2}{b_1^2}\right],\end{aligned} \tag{B5a}$$

$$\Omega_p^{\text{out2}}(x,t'') = \frac{|\Omega_{c2}|^2\Omega_p(0,0)\exp(id_{31}t_1)}{|\Omega_c|^2\sqrt{1-2iK_2(x-t''/K_1'')/\tau_0^2}}\exp\left\{iK_0(x-t''/K_1'') - \frac{\left[K_1(x-t''/K_1'') - T_{\text{off}_1}^2\right]^2}{[1-2iK_2(x-t''/K_1'')]/\tau_0^2}\right\}$$
$$+\frac{\Omega_{c2}\Omega_{M20}}{d_{31}}\left\{1-\exp\left[id_{31}\left(T_{\text{on}}^{M2}-T_{\text{off}}^{M2}\right)\right]\right\}\exp\left[-\frac{(x-a_2-t''/K_1'')^2}{b_2^2}\right], \tag{B5b}$$

where $t' = t - T_{\text{on}_1}^1$, $t'' = t - T_{\text{on}_1}^2$, $K_1' = \partial K'/\partial\omega$, and $K_1'' = \partial K''/\partial\omega$, with $K' = \frac{n_2^2\omega}{n_{\text{eff}}c} + \langle\frac{\kappa_{14}(z)(\omega+d_{21})}{|\zeta(z)\Omega_{c1}|^2-(\omega+d_{21})(\omega+d_{41})}\rangle$ and $K'' = \frac{n_2^2\omega}{n_{\text{eff}}c} + \langle\frac{\kappa_{14}(z)(\omega+d_{31})}{|\zeta(z)\Omega_{c2}|^2-(\omega+d_{31})(\omega+d_{41})}\rangle$. Here the waveform of incident probe field is assumed to be $\Omega_p(0,t)\tau_0 = \Omega_p(0,0)e^{-t^2/\tau_0^2}$, used as that in Fig. 3.

From Eq. (B5), we see that the microwave fields (proportional to Ω_{M10} and Ω_{M20}) used contribute indeed to the two retrieved (split) SP pulses. This is the reason why the SPBS quality can be improved by the application of the microwave fields.

APPENDIX C: DERIVATION OF THE NONLINEAR ENVELOPE EQUATION

To obtain the envelope equation governing the nonlinear evolution of the probe pulse based on the MB Eqs. (3) and (4), we take the asymptotic expansion [48]

$$\sigma_{jl} = \sigma_{jl}^{(0)} + \epsilon\sigma_{jl}^{(1)} + \epsilon^2\sigma_{jl}^{(2)} + \epsilon^3\sigma_{jl}^{(3)} + \cdots, \tag{C1a}$$
$$\Omega_p = \epsilon\Omega_p^{(1)} + \epsilon^2\Omega_p^{(2)} + \epsilon^3\Omega_p^{(3)} + \cdots, \tag{C1b}$$

where $\sigma_{jl}^{(0)} = \delta_{j0}\delta_{l0}$ the initial-state solution before the probe field is applied, and ϵ is a dimensionless small parameter characterizing the typical amplitude of the probe field. To have a divergence-free expansion, all terms on the right-hand side of the expansion (C1) are considered as functions of the multiscale variables $z_l = \epsilon^l z$ $(l = 0, 1, 2)$, $t_l = \epsilon^l t$ $(l = 0, 1)$ [48]. Substituting such expansion to the MB Eqs. (3) and (4), we obtain a set of equations which can be solved order by order.

At the first order of the expansion, we obtain the solution

$$\Omega_p^{(1)} = F\ \exp(i\theta), \tag{C2a}$$
$$\sigma_{21}^{(1)} = |\zeta(z)|^2[\Omega_{c1}^*(\omega+d_{31})/D]F\ \exp(i\theta), \tag{C2b}$$
$$\sigma_{31}^{(1)} = |\zeta(z)|^2[\Omega_{c2}^*(\omega+d_{21})/D]F\ \exp(i\theta), \tag{C2c}$$
$$\sigma_{41}^{(1)} = -[(\omega+d_{21})(\omega+d_{31})/D]\zeta(z)F\ \exp(i\theta), \tag{C2d}$$

where $D = -|\zeta(z)\Omega_{c1}|^2(\omega+d_{31}) - |\zeta(z)\Omega_{c2}|^2(\omega+d_{21}) + (\omega+d_{41})(\omega+d_{21})(\omega+d_{31})$, F is the envelope function of the slow variables z_1, z_2, and t_1, and $\theta = K(\omega)z_0 - \omega t_0$ with $K(\omega)$ the linear dispersion relation given by (5).

At the second order, we obtain the equation

$$i\left(\frac{\partial F}{\partial z_1} + \frac{1}{V_g}\frac{\partial F}{\partial t_1}\right) = 0, \tag{C3}$$

where $V_g \equiv (\partial K/\partial\omega)^{-1}$ is the group velocity of the probe pulse. Explicit expressions of the solution at this order are given by $\sigma_{j1}^{(2)} = a_{j1}^{(2)} i\frac{\partial}{\partial t_1}\zeta(z)F\ \exp(i\theta)$ $(j = 2, 3, 4)$, $\sigma_{42(43,32)}^{(2)} = a_{42(43,32)}^{(2)}|\zeta(z)F|^2\exp(-2\bar{\alpha}z_2)$ $(\bar{\alpha} = \epsilon^{-2}\alpha$ $[\alpha \equiv \text{Im}(K)]$ is the absorption coefficient), and $\sigma_{jj}^{(2)} = a_{jj}^{(2)}|\zeta(z)F|^2\exp(-2\bar{\alpha}z_2)$ $(j = 1, 2, 3, 4)$, with

$$a_{41}^{(2)} = \frac{1}{\kappa_{41}}\left(\frac{1}{V_g} - \frac{1}{c}\right), \tag{C4a}$$
$$a_{21}^{(2)} = -\frac{\zeta^*(z)\Omega_{c1}^*}{D^2}\left[(\omega+d_{31})^2(2\omega+d_{41}+d_{21}) + |\zeta(z)\Omega_{c2}|^2(d_{31}-d_{21})\right], \tag{C4b}$$
$$a_{31}^{(2)} = -\frac{\zeta^*(z)\Omega_{c2}^*}{D^2}[(\omega+d_{21})^2(2\omega+d_{41}+d_{31}) + |\zeta(z)\Omega_{c1}|^2(d_{21}-d_{31})], \tag{C4c}$$
$$a_{22}^{(2)} = \frac{-\Gamma_{34}X + \Gamma_{14}(B-B^*)}{\Gamma_{14}(A-A^*)}, \tag{C4d}$$
$$a_{33}^{(2)} = \frac{Q + i\Gamma_{14}|\zeta(z)\Omega_{c1}|^2(N^*-N)a_{22}^{(2)}}{i\Gamma_{14}P}, \tag{C4e}$$
$$a_{11}^{(2)} = \frac{X - i\Gamma_{14}\left(a_{22}^{(2)} + a_{33}^{(2)}\right)}{i\Gamma_{14}}, \tag{C4f}$$
$$a_{42}^{(2)} = \frac{M}{N}\left[\zeta^*(z)\Omega_{c2}^*\left(\frac{1}{i\Gamma_{14}}X + a_{33}^{(2)}\right) + a_{31}^{(1)}\right] - \frac{1}{N}\left[a_{21}^{*(1)} - \zeta(z)\Omega_{c1}\left(\frac{1}{i\Gamma_{14}}X + a_{22}^{(2)}\right)\right], \tag{C4g}$$
$$a_{43}^{(2)} = -\frac{M^*d_{32}^*}{\zeta^2(z)\Omega_{c1}\Omega_{c2}}\left[\zeta(z)\Omega_{c2}\left(\frac{1}{i\Gamma_{14}}X + a_{33}^{(2)}\right) + a_{31}^{*(1)} - \frac{\zeta^2(z)\Omega_{c1}\Omega_{c2}}{d_{32}^*}a_{42}^{*(2)}\right], \tag{C4h}$$
$$a_{32}^{(2)} = \frac{1}{d_{32}}\left(\zeta(z)\Omega_{c1}a_{43}^{*(2)} - \zeta^*(z)\Omega_{c2}^*a_{42}^{(2)}\right), \tag{C4i}$$

where

$$A = -\frac{d_{32}^* M^*}{\zeta^*(z)\Omega_{c1}^*}\left\{\frac{|\zeta(z)\Omega_{c1}|^2\zeta(z)\Omega_{c2}}{P}(N^*-N) - \frac{\zeta^2(z)\Omega_{c1}\Omega_{c2}}{d_{32}^* N^*}\left[\frac{M^*|\zeta(z)\Omega_{c1}|^2\zeta(z)\Omega_{c2}}{P}(N^*-N) - \zeta^*(z)\Omega_{c1}^*\right]\right\}, \quad \text{(C5a)}$$

$$B = \frac{d_{32}^* M^*}{\zeta^*(z)\Omega_{c1}^*}\left\{\zeta(z)\Omega_{c2}\frac{1}{i\Gamma_{14}}X + \frac{\zeta(z)\Omega_{c2}Q}{i\Gamma_{14}P} + a_{31}^{*(1)} - \frac{\zeta^2(z)\Omega_{c1}\Omega_{c2}}{d_{32}^* N^*}\left[M^*\zeta(z)\Omega_{c2}\left(\frac{1}{i\Gamma_{14}X} + \frac{Q}{i\Gamma_{14}P}\right)\right.\right.$$
$$\left.\left. + M^* a_{31}^{*(1)} - a_{21}^{(1)} - \zeta^*(z)\Omega_{c1}^*\frac{1}{i\Gamma_{14}}X\right]\right\}, \quad \text{(C5b)}$$

$$M = \frac{\zeta^2(z)\Omega_{c1}\Omega_{c2}}{d_{32}}\left(\frac{|\zeta(z)\Omega_{c1}|^2}{d_{32}} + d_{43}^*\right)^{-1}, \quad \text{(C5c)}$$

$$N = d_{42} + \frac{[\zeta^*(z)]^2\Omega_{c1}^*\Omega_{c2}^* M - |\zeta(z)\Omega_{c1}|^2}{d_{32}}, \quad \text{(C5d)}$$

$$P = N^* M\Omega_{c1}^*\Omega_{c2}^* - NM^*\Omega_{c1}\Omega_{c2}, \quad \text{(C5e)}$$

$$Q = [-i|N|^2\Gamma_{24} - P + |\zeta(z)\Omega_{c1}|^2(N^*-N)]X - i\Gamma_{14}\left[\zeta(z)\Omega_{c1}^* N^*\left(Ma_{31}^{(1)} - a_{21}^{*(1)}\right) - \text{c.c.}\right], \quad \text{(C5f)}$$

$$X = \frac{(\omega+d_{21})(\omega+d_{31})}{D} - \frac{(\omega+d_{21}^*)(\omega+d_{31}^*)}{D^*}. \quad \text{(C5g)}$$

With the solutions obtained above, we proceed to the third order of the expansion, and obtain the following envelope equation:

$$i\frac{\partial}{\partial z_2}F - \frac{1}{2}K_2\frac{\partial^2}{\partial t_1^2}F + W|F|^2F\,e^{-2\overline{\alpha}z_2} = 0, \quad \text{(C6)}$$

where $K_2 = \partial^2 K/\partial\omega^2$ is the coefficient of group-velocity dispersion and W is the coefficient of self-phase modulation, which reads

$$W = -\kappa_{41}\frac{S + \zeta(z)\left[\Omega_{c1}(\omega+d_{31})a_{42}^{*(2)} + \Omega_{c2}(\omega+d_{21})a_{43}^{*(2)}\right]}{D}, \quad \text{(C7)}$$

with $S = (\omega+d_{21})(\omega+d_{31})(2a_{11}^{(2)} + a_{22}^{(2)} + a_{33}^{(2)})$.

APPENDIX D: SOLITONIC CHARACTERS OF THE SPLIT NONLINEAR SPs AND THE DIFFERENCE BETWEEN THE TWO SPLIT SPs

The result in Fig. 5(c) shows that a surface polaritonic soliton can be split into two nonlinear SPs. Here we explain that these two retrieved nonlinear SPs can be approximately taken as solitons. The reasons are the following.

(i) The amplitudes of the two retrieved pulses have the same order of magnitude as that of the incident soliton before the storage, which means that the nonlinear effect in the retrieved two pulses plays the same role as that in the incident soliton. This point can also be seen by the propagation distance for the "soliton 1" and "soliton 2," which are both $x = 2.4$ mm, much larger than the nonlinear length ($L_{\text{NL}} = 0.79$ mm) of the system. That is to say, the nonlinear effect in the system has already played an important role in the retrieval process of the two pulses.

(ii) We know that the formation of a soliton requires the condition of the balance between dispersion and nonlinearity, unless a nonlinear pulse will be unstable during propagation [54]. From Fig. 5(c) we see that the retrieved two nonlinear pulses are stable during propagation, except for a small decay in amplitudes, which is due to the residual Ohmic loss in the metamaterial and the residual spontaneous emission and dephasing in the quantum emitters. Consequently, the two retrieved pulses can be approximately considered to be solitons (i.e., they are the outcome by the balance between the dispersion and the nonlinearity in the system). This point can also be understood clearly by comparing Fig. 5(c) with Fig. 4(c). In Fig. 4(c), the two retrieved pulses have large lowering in their amplitudes and large broadening in their widths, and hence they are not solitons. The physical reason is that, in the case of Fig. 4(c), the system works in a dispersion-dominant region where there is no nonlinearity to balance the dispersion of the system.

APPENDIX E: SPBS WORKING AT ROOM TEMPERATURE

Under a room-temperature environment, the inhomogeneous line broadening of the quantum emitters usually cannot be neglected, which might degrade the property of EIT [50] and hence the behavior of the SPBS. To illustrate this, we take a realistic example by selecting Pr:YSO as a dopant dielectric, where Pr^{3+} ions are doped into a layer near the metamaterial-dielectric interface [50]. A numerical simulation is carried out for a surface polaritonic soliton beam splitting by assuming, for simplicity, that the inhomogeneous line broadening is represented by modified parameters of the spontaneous emission and dephasing [55], i.e., $\Gamma_4 = 2\pi \times 0.16$ GHz, $\gamma_{21} = \gamma_{32} = \gamma_{32} = 2\pi \times 1.59$ kHz [50], with the other parameters being the same as those used in Sec. III D.

Shown in Fig. 7 is the result of the numerical simulation on the surface polaritonic soliton beam splitting realized by two optical excitation channels working at room temperature. One sees that, compared to Fig. 5, due to the existence of the inhomogeneous broadening decay of the soliton before and after the splitting is faster than that without the inhomogeneous

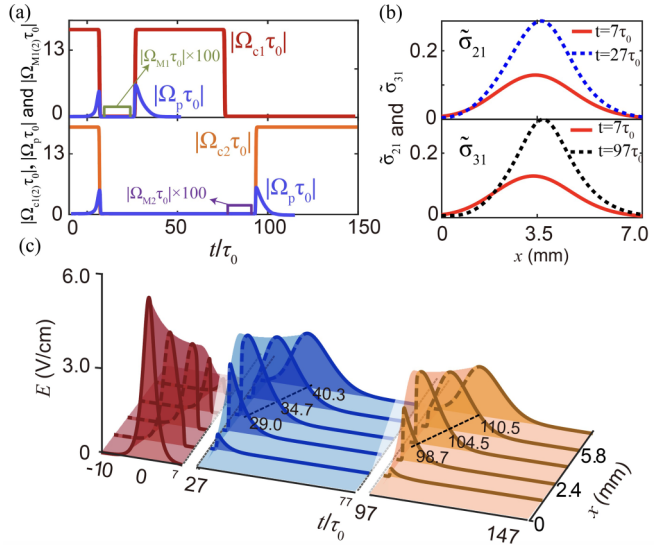

FIG. 7. Surface polaritonic soliton beam splitting realized by two optical excitation channels working at room temperature. (a) Timing sequences of the control fields and microwave fields [similar to Fig. 4(a)]. The solid blue lines are curves of the soliton pulse Ω_p during the storage (when Ω_{c1} and Ω_{c2} are switched off) and splitting (when Ω_{c1} and Ω_{c2} are switched on successively) at position $x = 3.50$ mm. (b) Coherences of the quantum emitters as functions of distance x at time $t = 7\tau_0$ (red solid line) and $t = 27\tau_0$ (blue dotted line) for $\tilde{\sigma}_{21}$, and $t = 7\tau_0$ (red solid line) and $t = 97\tau_0$ (black dotted line) for $\tilde{\sigma}_{31}$. (c) The electric field of the surface polaritonic soliton as a function of x and t during the splitting process (i.e., propagation, storage, and retrieval) of the SP.

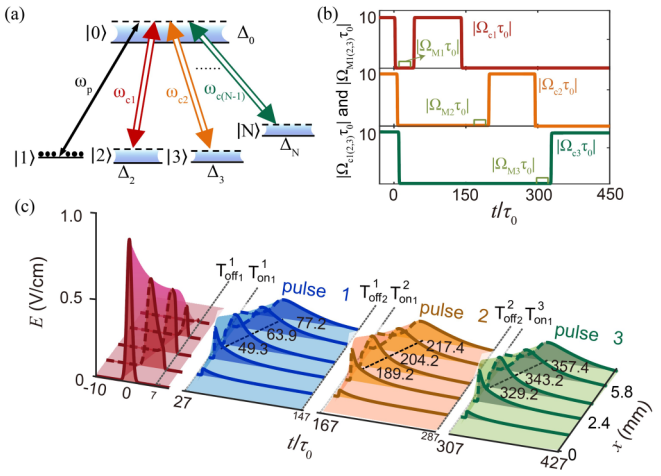

FIG. 8. SPBS with multiple excitation channels. (a) Excitation scheme of the quantum emitters with a N-pod type level configuration. (b) Timing sequences of the switching on and off there control fields (Ω_{c1}, Ω_{c2}, and Ω_{c3}), and the timing sequences of three microwave fields (Ω_{M1}, Ω_{M2}, and Ω_{M3}) in a quadripod type system. (c) The SP electric field as a function of x and t during the splitting process (i.e., propagation, storage, and retrieval) of the SP. A SP pulse (the leftmost part of the figure) can indeed be split into three SPs, i.e., the pulse 1, pulse 2, and pulse 3 in the figure.

broadening. As a result, the splitting efficiency of the soliton is lowered to $\eta = 64\%$.

APPENDIX F: SPBS THROUGH MULTIPLE EXCITATION CHANNELS

The scheme for realizing the SPBS with two excitation channels presented in the main text can be generalized to systems with more excitation channels. Shown in Fig. 8(a) is the level diagram and excitation scheme of the quantum emitters with an N-pod type level configuration, where the probe field (with angular frequency ω_p and half Rabi frequency Ω_p) couples the levels $|0\rangle$ and $|1\rangle$, and jth control field (with angular frequency ω_{cj} and half Rabi frequency Ω_{cj}) couples the levels $|0\rangle$ and $|j+1\rangle$ ($j = 1, \ldots, N-1$). Δ_0 is one-photon detuning and Δ_j is two-photon detuning ($j = 2, \ldots, N$).

To realize a SPBS in such a system, the control fields and the microwave fields must be switched off and on successively in a suitable way. For simplicity, here we consider only the case of a quadripod type system, with timing sequences of the switching on and off of three control fields (Ω_{c1}, Ω_{c2}, and Ω_{c3}) and the three microwave fields (Ω_{M1}, Ω_{M2}, and Ω_{M3}), as shown in Fig. 8(b). Figure 8(c) presents the result of a numerical simulation on the SPBS via such three excitation channels. We see that a SP pulse (the leftmost part of the figure) can indeed be split into three SPs, i.e., pulse1, pulse 2, and pulse 3 in the figure.

[1] R. Loudon, *The Quantum Theory of Light*, 3rd ed. (Oxford University, New York, 2000).

[2] M. O. Scully and M. S. Zubairy, *Quantum Optics* (Cambrige University, Cambridge, England, 2000).

[3] J.-W. Pan, Z.-B. Chen, C.-Y. Lu, H. Weinfurter, A. Zeilinger, and M. Żukowski, Multiphoton entanglement and interferometry, Rev. Mod. Phys. **84**, 777 (2012).

[4] C. Gardiner and P. Zoller, *The Quantum World of Ultar-Cold Atoms and Light Book II: The Physics of Quantu-Optical Devices* (Imperial College, London, 2015).

[5] Q. Gan, B. Guo, G. Song, L. Chen, Z. Fu, Y. J. Ding, and F. J. Bartoli, Plasmonic surface-wave splitter, Appl. Phys. Lett. **90**, 161130 (2007).

[6] J. Zhao, Y. Chen, and Y. Feng, Polarization beam splitting through an anisotropic metamaterial slab realized by a layered metal-dielectric structure, Appl. Phys. Lett. **92**, 071114 (2008).

[7] M. Rahm, D. A. Roberts, J. B. Pendry, and D. R. Smith, Transformation-optical design of adaptive beam bends and beam expanders, Opt. Express **16**, 11555 (2008).

[8] J. S. Q. Liu, R. A. Pala, F. Afshinmanesh, W. Cai, and M. L. Brongersma, A submicron plasmonic dichroic splitter, Nat. Commun. **2**, 525 (2011).

[9] S. Zhu, G. Q. Lo, and D. L. Kwong, Nanoplasmonic power splitters based on the horizontal nanoplasmonic slot waveguide, Appl. Phys. Lett. **99**, 031112 (2011).

[10] Y. J. Zhou and T. J. Cui, Multidirectional surface-wave splitters, Appl. Phys. Lett. **98**, 221901 (2011).

[11] J. Wang, X. Guan, Y. He, Y. Shi, Z. Wang, S. He, P. Holmström, L. Wosinski, L. Thylen, and D. Dai, Sub-μm^2 power splitters by using silicon hybrid plasmonic waveguides, Opt. Express **19**, 838 (2011).

[12] F. Lou, D. Dai, and L. Wosinski, Ultracompact polarization beam splitter based on a dielectric-hybrid plasmonic-dielectric coupler, Opt. Lett. **37**, 3372 (2012).

[13] S. Kumar, A. Huck, Y. Chen, and U. L. Andersen, Coupling of a single quantum emitter to end-to-end aligned silver nanowires, Appl. Phys. Lett. **102**, 103106 (2013).

[14] X. Zhang, Z. Li, J. Chen, S. Yue, and Q. Gong, A dichroic surface-plasmon-polariton splitter based on an asymmetric T-shape nanoslit, Opt. Express **21**, 14548 (2013).

[15] Y. Chen, G. Song, J. Xiao, L. Yu, and J. Zhang, Subwavelength polarization beam splitter with controllable splitting ratio based on surface plasmon polaritons, Opt. Express **21**, 314 (2013).

[16] P. V. Kapitanova, P. Ginzburg, F. J. Rodríguez-Fortuño, D. S. Filonov, P. M. Voroshilov, P. A. Belov, A. N. Poddubny, Y. S. Kivshar, G. A. Wurtz, and A. V. Zayats, Photonic spin Hall effect in hyperbolic metamaterials for polarization-controlled routing of subwavelength modes, Nat. Commun. **5**, 3226 (2014).

[17] J. Zheng, Z.-C. Ye, N.-L. Sun, R. Zhang, Z.-M. Sheng, H.-P. D. Shieh, and J. Zhang, Highly anisotropic metasurface: a polarized beam splitter and hologram, Sci. Rep. **4**, 6491 (2014).

[18] M. Khorasaninejad, W. Zhu, and K. B. Crozier, Efficient polarization beam splitter pixels based on a dielectric metasurface, Optica **2**, 376 (2015).

[19] Z. Fan, S. Li, Q. Liu, J. Li, and Y. Xie, Plasmonic polarization beam splitter based on dual-core photonic crystal fiber, Plasmonics **10**, 1283 (2015).

[20] R. Halir, P. Cheben, J. M. Luque-González, J. D. Sarmiento-Merenguel, J. H. Schmid, G. Wangüemert-Pérez, D.-X. Xu, S. Wang, A. Ortega-Moñux, and I. Molina-Fernández, Ultra-broadband nanophotonic beamsplitter using an anisotropic sub-wavelength metamaterial, Laser Photon. Rev. **10**, 1039 (2016).

[21] Z. Gao, F. Gao, and B. Zhang, Multi-directional plasmonic surface-wave splitters with full bandwidth isolation, Appl. Phys. Lett. **108**, 111107 (2016).

[22] Y. Wang, X. Hong, T. Sang, and G. Yang, Tunable 1×2 plasmonic splitter of dielectric-loaded graphene waveguide based on multimode interference, Appl. Phys. Express **9**, 125102 (2016).

[23] M. Papaioannou, E. Plum, and N. I. Zheludev, All-optical pattern recognition and image processing on a metamaterial beam splitter, ACS Photon. **4**, 217 (2017).

[24] M. Nikoufard, M. K. Alamouti, and S. Pourgholi, Multimode interference power-splitter using InP-based deeply etched hybrid plasmonic waveguide, IEEE Trans. Nanotechnol. **16**, 477 (2017).

[25] X. Zhang, R. Deng, F. Yang, C. Jiang, S. Xu, and M. Li, Metasurface-based ultrathin beam splitter with variable split angle and power distribution, ACS Photon. **5**, 2997 (2018).

[26] F. Gan, C. Sun, H. Li, Q. Gong, and J. Chen, On-chip polarization splitter based on a multimode plasmonic waveguide, Photon. Res. **6**, 47 (2018).

[27] F. Liu, T. Xu, S. Wang, Z. H. Hang, and J. Li, Polarization beam splitting with gauge field metamaterials, Adv. Opt. Mater. **7**, 1801582 (2019).

[28] Z. Liu, J. Guo, B. Tian, Y. Bian, R.-Y. Zhang, and Z. Wang, Omnidirectional polarization beam splitter for white light, Opt. Express **27**, 7673 (2019).

[29] T. Wang, M. Koštrun, and S. F. Yelin, Multiple beam splitter for single photons, Phys. Rev. A **70**, 053822 (2004).

[30] I. E. Mazets, Adiabatic pulse propagation in coherent atomic media with the tripod level configuration, Phys. Rev. A **71**, 023806 (2005).

[31] A. Raczyński, J. Zaremba, and S. Zielińska-Kaniasty, Beam splitting and Hong-Ou-Mandel interference for stored light, Phys. Rev. A **75**, 013810 (2007).

[32] Y. Xiao, M. Klein, M. Hohensee, L. Jiang, D. F. Phillips, M. D. Lukin, and R. L. Walsworth, Slow Light Beam Splitter, Phys. Rev. Lett. **101**, 043601 (2008).

[33] X.-L. Song, A.-J. Li, L. Wang, Z.-H. Kang, J. Kou, B. Zhang, C.-L. Wang, Y. Jiang, and J.-Y. Gao, Storage and switching of multiple optical signals among three channels, Phys. Rev. A **79**, 053857 (2009).

[34] Y. Zhang, C. Zuo, H. Zheng, C. Li, Z. Nie, J. Song, H. Chang, and M. Xiao, Controlled spatial beam splitter using four-wave-mixing images, Phys. Rev. A **80**, 055804 (2009).

[35] H. Wang, S. Li, Z. Xu, X. Zhao, L. Zhang, J. Li, Y. Wu, C. Xie, K. Peng, and M. Xiao, Quantum interference of stored dual-channel spin-wave excitations in a single tripod system, Phys. Rev. A **83**, 043815 (2011).

[36] K. F. Reim, J. Nunn, X.-M. Jin, P. S. Michelberger, T. F. M. Champion, D. G. England, K. C. Lee, W. S. Kolthammer, N. K. Langford, and I. A. Walmsley, Multipulse Addressing of a Raman Quantum Memory: Configurable Beam Splitting and Efficient Readout, Phys. Rev. Lett. **108**, 263602 (2012).

[37] D.-S. Ding, J.-H. Wu, Z.-Y. Zhou, B.-S. Shi, X.-B. Zou, and G.-C. Guo, Multiple image storage and frequency conversion in a cold atomic ensemble, Phys. Rev. A **87**, 053830 (2013).

[38] M.-J. Lee, J. Ruseckas, C.-Y. Lee, V. Kudriašov, K.-F. Chang, H.-W. Cho, G. Juzeliūnas, and I. A. Yu, Experimental demonstration of spinor slow light, Nat. Commun. **5**, 5542 (2014).

[39] S.-J. Yang, X.-H. Bao, and J.-W. Pan, Modulation of single-photon-level wave packets with two-component electromagnetically induced transparency, Phys. Rev. A **91**, 053805 (2015).

[40] C. Shou and G. Huang, Slow-light soliton beam splitters, Phys. Rev. A **99**, 043821 (2019).

[41] M. Fleischhauer, A. Imamoglu, and J. P. Marangos, Electromagnetically induced transparency: Optics in coherent media, Rev. Mod. Phys. **77**, 633 (2005).

[42] A. Kamli, S. A. Moiseev, and B. C. Sanders, Coherent Control of Low Loss Surface Polaritons, Phys. Rev. Lett. **101**, 263601 (2008).

[43] C. Tan and G. Huang, Surface polaritons in a negative-index metamaterial with active Raman gain, Phys. Rev. A **91**, 023803 (2015).

[44] J. Su, D. Xu, and G. Huang, Storage and retrieval of surface polaritons, ACS Photon. **5**, 2496 (2018).

[45] The quantum emitters can be quantum dots, nitrogen-valence centers in diamond, rare-earth ions in crystals, or similar [42–44].

[46] For simplicity, we assume the incident electric field has a large width in y direction so that all quantities are independent of y.

[47] ω is a deviation (sideband) frequency of the SP, generated by the interaction between the probe pulse and the metamaterial-dielectric interafce with the quantum emitters. Thus the frequency and wave number of the SP are given by $\omega_p + \omega$ and $k_p + K_p(\omega)$, respectively.

[48] G. Huang, L. Deng, and M. G. Payne, Dynamics of ultraslow optical solitons in a cold three-state atomic system, Phys. Rev. E **72**, 016617 (2005).

[49] The Hamiltonian of the system in the presence of the microwave fields is presented in Appendix A.

[50] E. Kuznetsova, O. Kocharovskaya, P. Hemmer, and M. O. Scully, Atomic interference phenomena in solids with a long-lived spin coherence, Phys. Rev. A **66**, 063802 (2002).

[51] K. Lemr, K. Bartkiewicz, A. Cernoch, and J. Soubusta, Resource-efficient linear-optical quantum router, Phys. Rev. A **87**, 062333 (2013).

[52] M. Ahumada, P. A. Orellana, F. Domínguez-Adame, and A. V. Malyshev, Tunable single-photon quantum router, Phys. Rev. A **99**, 033827 (2019).

[53] The scheme suggested here can be generalized to the case of the SP working at single-photon level, for which, however, a complete quantum approach for both the emitters and the SP field must be adopted, which will be considered elsewhere.

[54] M. J. Ablowitz, *Nonlinear Dispersive Waves: Asymptotic Analysis and Solitons* (Cambridge University Press, Cambridge, UK, 2011).

[55] C. Hang and G. Huang, Weak-light superluminal vector solitons in a room-temperature four-level active-Raman-gain medium, J. Opt. Soc. Am. B **26**, 413 (2009).